

High Molar Extinction Coefficient Heteroleptic Ruthenium Complexes for Thin Film Dye-Sensitized Solar Cells

Daibin Kuang, Seigo Ito, Bernard Wenger, Cedric Klein, Jacques-E Moser, Robin Humphry-Baker, Shaik M. Zakeeruddin,* and Michael Grätzel*

Contribution from the Laboratory for Photonics and Interfaces, Institute of Chemical Sciences and Engineering, Ecole Polytechnique Fédérale de Lausanne, 1015 Lausanne, Switzerland

Received December 16, 2005; E-mail: shaik.zakeer@epfl.ch; michael.gratzel@epfl.ch

Abstract: Two novel heteroleptic sensitizers, Ru((4,4-dicarboxylic acid-2,2'-bipyridine)(4,4'-bis(*p*-hexyloxy-styryl)-2,2'-bipyridine)(NCS)₂ and Ru((4,4-dicarboxylic acid-2,2'-bipyridine)(4,4'-bis(*p*-methoxystyryl)-2,2'-bipyridine)(NCS)₂, coded as K-19 and K-73, respectively, have been synthesized and characterized by ¹H NMR, FTIR, UV-vis absorption, and emission spectroscopy and excited-state lifetime and spectroelectrochemical measurements. The introduction of the alkoxy-styryl group extends the conjugation of the bipyridine donor ligand increasing markedly their molar extinction coefficient and solar light harvesting capacity. The dynamics of photoinduced charge separation following electronic excitation of the K-19 dye was scrutinized by time-resolved laser spectroscopy. The electron transfer from K-19 to the conduction band of TiO₂ is completed within 20 fs while charge recombination has a half-life time of 800 μs. The high extinction coefficients of these sensitizers enable realization of a new generation of a thin film dye sensitized solar cell (DSC) yielding high conversion efficiency at full sunlight even with viscous electrolytes based on ionic liquids or nonvolatile solvents. An unprecedented yield of over 9% was obtained under standard reporting conditions (simulated global air mass 1.5 sunlight at 1000 W/m² intensity) when the K-73 sensitizer was combined with a nonvolatile "robust" electrolyte. The K-19 dye gave a conversion yield of 7.1% when used in conjunction with the binary ionic liquid electrolyte. These devices exhibit excellent stability under light soaking at 60 °C. The effect of the mesoscopic TiO₂ film thickness on photovoltaic performance has been analyzed by electrochemical impedance spectroscopy (EIS).

Introduction

Following its discovery in 1991,¹ research on the dye-sensitized solar cell (DSC) has progressed remarkably, rendering it a credible chemical alternative to solid-state silicon based devices.^{2–5} The high efficiency of the DSC arises from the collective effect of numerous well-tuned physical-chemical properties, the key issue being the panchromatic sensitization of large band-gap mesoscopic semiconductor electrodes. Ruthenium polypyridyl complexes such as the *cis*-Ru(SCN)₂L₂ (L = 2,2'-bipyridyl-4,4'-dicarboxylate (N3) or the black dye Ru-

(SCN)₃L (L = 4,4',4''-tricarboxy-2,2':6',2''-terpyridine)⁶ showed the best performance as sensitizers so far due to their advantageous spectral properties and high stability. While more than 11% conversion efficiency has been reached with the N3 dye, a film thickness of over 15 microns and a volatile redox electrolyte were required to achieve this performance. The long-term containment at elevated temperatures of the volatile solvent mixture employed still remains a major challenge.⁷

This dilemma is currently being addressed by the development of novel sensitizers with an increased optical cross section allowing thinner TiO₂ films and nonvolatile electrolytes to be employed. A successful approach has been to replace one of the 2,2'-bipyridyl-4,4'-dicarboxylate groups in the N3 dye by a styryl-substituted bipyridine. This not only increases the extinction coefficient of the sensitizer by extending the π-conjugation of the ligand but also augments its hydrophobicity, preventing dye desorption by water and stabilizing device performance under long-term light soaking and thermal stress.

Following our recent communication on the K-19 dye Ru((4,4'-dicarboxylic acid-2,2'-bipyridine)(4,4'-bis(*p*-hexyloxy-styryl)-

- (1) O'Regan, B.; Grätzel, M. *Nature* **1991**, *353*, 737.
- (2) (a) Benkstein, K. D.; Kopidakis, N.; van de Lagematt, J. Frank, A. J. *J. Phys. Chem. B* **2003**, *7759*. (b) Benkő, G.; Skárman, B.; Wallenberg, R.; Hagfeldt, A.; Sundström, V.; Yartsev, A. P. *J. Phys. Chem. B* **2003**, *107*, 1370. (c) Nakade, S.; Saito, Y.; Kubo, W.; Kitamura, T.; Wada, Y.; Yanagida, S. *J. Phys. Chem. B* **2003**, *107*, 8607.
- (3) (a) Grätzel, M. *Chem. Lett.* **2005**, *34*, 8–13. (b) Yanagida, M.; Yamaguchi, T.; Kurashige, M.; Fujihashi, G.; Hara, K.; Katoh, R.; Sugihara, H.; Arakawa, H. *Inorg. Chim. Acta* **2003**, *351*, 283. (c) Heimer, T. A.; Heilweil, E. J.; Bignozzi, C. A.; Meyer, G. J. *J. Phys. Chem. A* **2000**, *104*, 4256.
- (4) Adachi, M.; Murata, Y.; Takao, J.; Jiu, J.; Sakamoto, M.; Wang, F. *J. Am. Chem. Soc.* **2004**, *126*, 14943. (b) Ushiroda, S.; Ruzycski, N.; Lu, Y.; Spitzer, M. T.; Parkinson, B. A. *J. Am. Chem. Soc.* **2005**, *127*, 5158.
- (5) For example, see: (a) Wang, P.; Zakeeruddin, S. M.; Moser, J. E.; Humphry-Baker, R.; Grätzel, M. *J. Am. Chem. Soc.* **2004**, *126*, 7164. (b) Sapp, S. A.; Elliott, M.; Contado, C.; Caramori, S.; Bignozzi, C. A. *J. Am. Chem. Soc.* **2002**, *124*, 11215. (c) Nusbaumer, H.; Zakeeruddin, S. M.; Moser, J.-E.; Grätzel, M. *Chem.—Eur. J.* **2003**, *9*, 3756. (d) Balzani, V.; Campagna, S.; Dentì, G.; Juris, A.; Serroni, S.; Venturi, M. *Acc. Chem. Res.* **1998**, *31*, 26. (e) Hara, K.; Kurashige, M.; Dan-oh, Y.; Kasada, C.; Shinpo, A.; Suga, S.; Sayama, K.; Arakawa, H. *New J. Chem.* **2003**, 783. (f) Horiuchi, T.; Miura, H.; Uchida, S. *Chem. Commun.* **2003**, 3036.

- (6) (a) Nazeeruddin, M. K.; Pechy, P.; Renouard, T.; Zakeeruddin, S. M.; Humphry-Baker, R.; Liska, P.; Cevey, L.; Costa, E.; Shklover, V.; Spiccia, L.; Deacon, G. B.; Bignozzi, C. A.; Grätzel, M. *J. Am. Chem. Soc.* **2001**, *123*, 1613. (b) Nazeeruddin, M. K.; Kay, A.; Rodicio, I.; Humphry-Baker, R.; Müller, E.; Liska, P.; Vlachopoulos, N.; Grätzel, M. *J. Am. Chem. Soc.* **1993**, *115*, 6382.
- (7) Grätzel, M. *Inorg. Chem.*, **2005**, *44* (20), 6841.

2,2'-bipyridine)(NCS)₂,⁸ an in-depth analysis of this promising new generation of sensitizers is performed in the present study. This includes a comparison of the K-19 with its less hydrophobic analogue Ru(4,4-dicarboxylic acid-2,2'-bipyridine)(4,4'-bis(*p*-methoxystyryl)-2,2'-bipyridine)(NCS)₂ coded as K-73, where the hexyl chains are replaced by methyl groups.

Experimental Section

Reagents. The high molar extinction coefficient sensitizer K-19, Ru(4,4-dicarboxylic acid-2,2'-bipyridine)(4,4'-bis(*p*-hexyloxystyryl)-2,2'-bipyridine)(NCS)₂ was synthesized as reported earlier.⁸ The molecular structures of sensitizer K-19 and K-73 are shown in Figure S1. Ionic liquids including 1-propyl-3-methylimidazolium iodide (PMII), 1-ethyl-3-methylimidazolium bis(trifluoromethylsulfonyl)imide (EMITFSI), and 1-ethyl-3-methylimidazolium thiocyanate (EMINCS) were prepared according to literature methods, and their purities were confirmed by ¹H NMR spectra.⁹ The coadsorbents 3-phenylpropionic acid (PPA) and guanidinium thiocyanate (GuNCS) were purchased from Aldrich, and 1-decylphosphonic acid (DPA) from Lancaster was used as received. *N*-Methylbenzimidazole (NMBI, from Aldrich) was recrystallized from diethyl ether before use.

Synthesis of 4,4'-Bis(2-(4-methoxyphenyl)styryl)-2,2'-bipyridine. Solid *tert*-BuOK (7.5 g, 67 mmol) was added to a solution of 4,4'-dimethyl-2,2'-bipyridine (3.0 g, 16 mmol) and 4-methoxybenzaldehyde (5.5 g, 40 mmol) in anhydrous DMF (100 mL). The resulting mixture was stirred 24 h at room temperature under nitrogen. The solvent was evaporated, and methanol (200 mL) was added. The insoluble solid was filtered on a sintered crucible and recrystallized from hot acetic acid, filtered, and washed with methanol to obtain the desired product as a beige solid (4 g, 58%).

Synthesis of Ru(4,4'-bis(2-(4-methoxyphenyl)styryl)-2,2'-bipyridine)(*p*-cymene)(Cl)₂. A mixture of 4,4'-bis(2-(4-methoxyphenyl)styryl)-2,2'-bipyridine (0.5 g, 1.2 mmol) ligand and [Ru(Cl)₂(*p*-cymene)]₂ (0.365 g, 0.59 mmol) in ethanol (80 mL) was refluxed for 4 h under nitrogen. After evaporation of the solvent, pure Ru(4,4'-bis(2-(4-methoxyphenyl)styryl)-2,2'-bipyridine)(*p*-cymene)(Cl)₂ complex was left as an orange colored oil. ¹H NMR (200 MHz, 25 °C, CDCl₃) δ 0.83 (s, 3H), 0.87 (s, 3H), 2.16 (s, 3H), 2.35 (m, 1H), 3.66 (s, 6H), 5.84 (d, *J* = 5.8 Hz, 2H), 5.92 (d, *J* = 5.8 Hz, 2H), 6.75 (m, 6H), 7.36 (d, *J* = 5.5 Hz, 2H), 7.51 (d, *J* = 8.5 Hz, 4H), 7.74 (d, *J* = 16 Hz, 2H), 8.57 (s, 2H), 9.23 (d, *J* = 5.5 Hz, 2H).

Ru(4,4'-bis(2-(4-methoxyphenyl)styryl)-2,2'-bipyridine)(4,4'-dicarboxy-2,2'-bipyridine)(NCS)₂. A Ru(4,4'-bis(2-(4-methoxyphenyl)styryl)-2,2'-bipyridine)(*p*-cymene)(Cl)₂ and 4,4'-dicarboxy-2,2'-bipyridine (0.291 g, 1.2 mmol) in DMF (60 mL) were heated to 140 °C for 4 h under nitrogen in the dark. To the green reaction mixture was then added NH₄NCS (2 g, 26 mmol), and the heating was continued for another 4 h. The reaction mixture was cooled to room temperature, and after the DMF was evaporated, water (200 mL) was added and the resulting purple solid was filtered and washed with water. The crude compound was dissolved in basic methanol (tetrabutylammonium hydroxide) solution and purified by passing through a Sephadex LH-20 column with methanol as the eluent. After collecting the main band and evaporating the solvent, the resultant solid was redissolved in water and the pH was lowered to 4.8 by titrating with dilute nitric acid to obtain the K-73 complex, containing one proton and one tetrabutylammonium cation (TBA⁺), as a precipitate. The final product was washed thoroughly with water and dried under a vacuum. ¹H NMR (δ_H/ppm in CD₃OD + NaOD) 9.45 (d, 1H), 9.20 (d, 1H), 8.95 (s, 1H), 8.80 (s, 1H), 8.30 (s, 1H), 8.15 (s, 1H), 8.00 (d, 1H), 7.90 to 6.80 (m,

18H), 4.05 (s, 3H), 4.0 (s, 3H), 3.2 (t, 8H), 2.8 to 1 (m, 28H). Anal. Calcd for RuC₅₈H₆₇N₇O₆S₂: C, 62.01; H, 6.01; N, 8.73%. Found: C, 62.37; H, 6.35; N, 8.6%.

Instrumentation. ¹H NMR spectra were measured on a Bruker 200 MHz spectrometer. The ¹H spectra were referenced to tetramethylsilane. Elemental analysis was carried out at the Institute of Chemical Science and Engineering at the EPFL. UV-vis and photoluminescence spectra were measured using a 1-cm path length quartz cell and a Cary 5 spectrophotometer or Spex Fluorolog 112 spectrofluorometer, respectively. The emitted light was detected with a Hamamatsu R2658 photomultiplier operated in the single-photon counting mode. The emission spectrum was photometrically corrected with a calibrated 200 W tungsten lamp as the reference source.

ATR-FTIR Measurements. The spectra for all the samples were measured using a Digilab FTS 7000 FTIR spectrometer fitted with a DTGS detector. All the data reported here were taken with the "Golden Gate" 45° diamond anvil ATR accessory. Spectra were derived from 64 scans at a resolution of 2 cm⁻¹. Prior to measuring the spectra, the dyed films were rinsed with acetonitrile solvent to washout any weakly adsorbed molecules and dried.

Electrochemical Impedance Measurements. Impedance spectra of fully assembled DSCs having different film thicknesses were measured in the dark at -0.68 V applied forward bias or under simulated AM1.5 global illumination (450 W xenon lamp equipped with appropriate filters) at open circuit using a computer controlled potentiostat (EG&G, M273) equipped with a frequency response analyzer (EG&G, M1025). The spectra were scanned in a frequency range of 0.005 Hz–100 kHz at room temperature with an alternating voltage amplitude set at 10 mV.

Oxidation of Sensitizer. Electrochemical oxidation was carried out with a three-electrode spectroelectrochemical cell. TBAPF₆ (0.1 M) dissolved in acetonitrile was used as the electrolyte. The electrode potential was adjusted by a PC-controlled AutoLab PSTAT10 electrochemical workstation (Eco Chimie). The UV-vis spectra were recorded by polarizing the electrode at 0.8 V vs NHE until the current drops to 1/10 of the initial value.

Femtosecond Transient Spectrometer. A detailed description of the setup used for time-resolved transient absorption measurements has been given in a previous paper.¹⁰ Briefly, the system is based on a Ti:sapphire amplified fiber laser source (Clark-MXR CPA 2001) providing pulses at a 1 kHz repetition rate centered at 775 nm with a duration of 120 fs and a pulse energy of 1 mJ. One part of the beam is used to pump a noncollinear parametric amplifier (NOPA) to produce the pump pulse centered at 520 nm with a typical duration of 30 fs after compression. The supercontinuum probe is generated by focusing a small part of the fundamental beam (<3 μJ) in a 2 mm sapphire plate. The white light continuum was collimated with a parabolic mirror, split into a probe and reference beam with a thin metallic beam splitter, and focused on the sample with another parabolic mirror in order to minimize chirp. The energy of the pump beam was reduced to 1 μJ before focusing on the sample, and the relative polarization of the beams was adjusted at the magic angle. The reference and signal beams were analyzed in a spectrograph (Triax 320, Jobin-Yvon) and detected by a double photodiode array with each 1024 elements (Princeton Instruments).

In the two-color pump-probe scheme, parts of the fundamental beam are used to pump two independent NOPAs that are tuned in order to provide pulses centered at 535 nm for the pump and 890 nm for the probe. After compression, the laser beams are focused on the sample by fused silica lenses. Neutral density filters are used to ensure intensity-independent dynamics. To avoid dye degradation, the sample is constantly rotated. For detection, the signal of a photoreceiver (Nirvana 2007, New Focus) is sent to a lock-in amplifier (SR-830, Stanford Research Instruments) tuned at the frequency of a chopper selecting one pulse over two (500 Hz).

(10) Pelet, S.; Grätzel, M.; Moser, J. E. *J. Phys. Chem. B* **2003**, *107*, 3215.

(8) (a) Wang, P.; Klein, C.; Humphry-Baker, R.; Zakeeruddin, S. M.; Grätzel, M. *J. Am. Chem. Soc.* **2005**, *127*, 808. (b) Wang, P.; Klein, C.; Humphry-Baker, R.; Zakeeruddin, S. M.; Grätzel, M. *Appl. Phys. Lett.* **2005**, *86*, 123508.

(9) Pringle, J. M.; Golding, J.; Forsyth, C. M.; Deacon, G. B.; Forsyth, M.; MacFarlane, D. R. *J. Mater. Chem.* **2002**, *12*, 3475.

The samples were made of 8 μm thick TiO_2 films soaked overnight in a 0.3 mM K-19 dye solution in a 1:1 mixture of *t*-BuOH/ CH_3CN . After dye absorption the films were covered with the redox inactive ionic liquid (1-ethyl-3-methylimidazolium bis(trifluoromethylsulfonyl)imide) or when indicated, with the nonvolatile electrolyte described below. The optical densities of the films were typically 2.0 at 527 nm. Al_2O_3 films were prepared as previously described,¹¹ and dye adsorption was accomplished following the same procedure as that for TiO_2 .

Nanosecond Laser Transient Absorbance Measurements. Dye-coated, 8 μm thick transparent nanocrystalline TiO_2 films were excited by nanosecond laser pulses produced by a broad-band optical parametric oscillator (OPO GWU-355), pumped by a frequency-tripled Q-switched Nd:YAG laser (Continuum Powerlite 7030). Excitation pulses ($\lambda = 600$ nm, 30 Hz repetition rate, pulse width at half-height of 7 ns) were attenuated by neutral density filters to reduce pulse fluence on the sample down to 25 $\mu\text{J cm}^{-2}$. The probe light from a Xe arc lamp was passed through a monochromator, various optical elements, the sample, and a second monochromator before being detected by a fast photomultiplier tube. Typically, averaging over 3000 laser shots was necessary to get satisfactory signal/noise levels.

Preparation of Mesoscopic TiO_2 Films. The mesoscopic TiO_2 film used as photoanode consisted of two layers. A transparent, high surface area layer of 20 nm TiO_2 particles was first printed on the fluorine-doped SnO_2 (FTO) conducting glass electrode obtained from LOF (TEC-15, sheet resistance 15 Ohm/square). Subsequently a second layer of 400 nm light scattering anatase particles was applied as reported,¹² with some modifications as explained below. The FTO glass was washed with ethanol and treated by UV- O_3 for 20 min in order to remove organics or contaminants. Thereafter it was placed in a 40 mM TiCl_4 aqueous solution at 70 $^\circ\text{C}$ for 30 min to enhance adhesion between the TiO_2 particles and the FTO surface. The transparent TiO_2 film of 3.4 μm thickness (particle size: 20 nm) was screen-printed on the clean FTO glass as described above. A thicker transparent TiO_2 layer can be obtained by repeating the operation. Thinner films (1 or 2 μm) were made by a similar procedure using a diluted TiO_2 paste. In the present study, film thicknesses of 1, 2, 3.4, 6.8, 10.2, and 13.6 μm were investigated. To enhance light harvesting in the red and near-IR spectral region, another layer was screen-printed by using a paste of 400 nm light scattering TiO_2 particles. The thickness of the scattering layer was kept constant at 4 μm . The layer thickness was determined by using an Alpha-Step 200 Surface Profilometer (Tencor Instruments, USA). The double layer composed of the transparent and light scattering particle was gradually heated to 500 $^\circ\text{C}$ and sintered for 15 min. The sintered double films were further treated with 40 mM TiCl_4 aqueous solution at 70 $^\circ\text{C}$ for 30 min, then washed with water and ethanol, and stored in dry air prior to device fabrication. The porosity and pore size of the TiO_2 paste used for the transparent layer as characterized by Gemini 2327 nitrogen adsorption apparatus (Micromeritics Instrument Corp., USA) were 63% and 22 nm, respectively.

Fabrication of DSC Devices. The double layer films were heated to 520 $^\circ\text{C}$ and sintered for 30 min, then cooled to ~ 80 $^\circ\text{C}$ and immersed into the dye solution at room temperature for 16 h. The dye solution containing 300 μM K-19 or K-73 in acetonitrile and *tert*-butyl alcohol (volume ratio: 1:1) was used to sensitize the photoanode. In the presence of coadsorbent, 300 μM PPA or 75 μM DPA was added to the above dye solution. Dye coated double layer films were assembled and sealed with a thin transparent hot-melt 25 μm thick Surlyn ring (DuPont) to the counter electrodes (Pt on FTO glass, chemical deposition of 0.05 M hexachloroplatinic acid in 2-propanol at 400 $^\circ\text{C}$ for 15 min). The electrolyte was injected into the interelectrode space

from the counter electrode side through a predrilled hole, and then the hole was sealed with a Bynel sheet and a thin glass slide cover by heating. The nonvolatile electrolyte contains 0.8 M PMII, 0.15 M iodine, 0.1 M GuNCS, and 0.5 M NMBI in 3-methoxypropionitrile. The solvent-free ionic liquid electrolyte contains 0.2 M iodine, 0.5 M NMBI, and 0.1 M GuNCS in a mixture of PMII/EMINCS (13:7 vol ratio).

Photocurrent–Voltage Measurements. The irradiation source for the photocurrent–voltage (I – V) measurement is a 450 W xenon light source (Osram XBO 450, USA), which simulates the solar light. The incident light intensity was calibrated with a standard Si solar cell. The spectral output of the lamp matched precisely the standard global AM 1.5 solar spectrum in the region 350–750 nm (mismatch < 2%) by the aid of a Schott K113 Tempax sunlight filter (Präzisions Glas & Optik GmbH, Germany). Various irradiance intensities (from 0.01 to 1.0 sun) can be provided with neutral wire mesh attenuators. The current–voltage curves were obtained by measuring the photocurrent of the cells using a Keithley model 2400 digital source meter (Keithley, USA) under an applied external potential scan. The transient current dynamics characterization of the cell was obtained using the same system of I – V measurement. The measurement of incident photon-to-current conversion efficiency (IPCE) was performed by a similar data collecting system but under monochromatic light. IPCE was plotted as a function of excitation wavelength. The incident light from a 300 W xenon lamp (ILC Technology, USA) was focused through a Gemini-180 double monochromator (Jobin Yvon Ltd., UK) onto the cell under test.

Light-Soaking Stability. Hermetically sealed cells were used to check the long-term stability under thermal stress (60 $^\circ\text{C}$) and visible light soaking. The cells were covered with a polymer film of 50 μm thickness (Preservation Equipment Ltd, UK), which acts as a UV cutoff filter, and were illuminated at open circuit under a Suntest CPS lamp (ATLAS GmbH, 100 mW/cm^2 , 60 $^\circ\text{C}$). The cells were taken out at regular intervals to record the photocurrent–voltage curve measured over a period of 1000 h.

Results and Discussion

1. Molecular Orbital Calculations. The Spartan commercial software was used to calculate the molecular orbitals of the K-73 heteroleptic ruthenium sensitizers and thereby the photoconversion efficiency. The profiles for the highest occupied molecular orbital (HOMO) and lowest unoccupied molecular orbital (LUMO) are presented in Figure S2. The LUMO is localized on the 4,4'-COOH 2,2'-bipyridine with the electron density being highest on the oxygen atoms of the carboxylate groups while the HOMO is shared by the Ru and NCS ligands.

2.1. Redox Potential. Cyclic voltammetry was performed to measure the redox potential of the sensitizer K-73 and the result are shown in Figure S3. For the K-73 dye adsorbed on the TiO_2 film, the average of the peak potentials of the cathodic and anodic wave was at 1.01 V vs. normal hydrogen electrode (NHE). This value is about 0.6 V more positive than the potential of the iodide/triiodide couple in the redox electrolyte providing a large driving force for the dye regeneration and thus net charge separation.

2.2. Electronic, Emission Spectra, and Exited State Lifetime. The two heteroleptic ruthenium complexes, K-19 and K-73, exhibit two intense broad absorption bands in the visible region at 410 and 545 nm due to metal-to-ligand charge-transfer (MLCT) transitions (Figure S4). In addition there are two features in the UV region. As observed in K-19 dye,^{8a} the narrow band at 310 nm arises from the π – π^* transition of the 4,4'-dicarboxy 2,2'-bipyridine ligand, and the broad band at 350 nm

(11) Nüesch, F.; Shklover, V.; Moser, J. E.; Grätzel, M. *J. Am. Chem. Soc.* **1996**, *118*, 5420.

(12) (a) Barbé, C. J.; Arendse, F.; Comte, P.; Jirousek, M.; Lenzmann, F.; Shklover, V.; Grätzel, M. *J. Am. Ceram. Soc.* **1997**, *80*, 3157. (b) Wang, P.; Zakeeruddin, S. M.; Comte, P.; Charvet, R.; Humphry-Baker, R.; Grätzel, M. *J. Phys. Chem. B* **2003**, *107*, 14336.

is assigned to the $\pi-\pi^*$ transition of the 4,4'-bis(2-(4-methoxyphenyl)styryl)-2,2'-bipyridine having an extended π system.

The light harvesting efficiency is primarily governed by the molar extinction coefficient of the dye. For Z 907Na dye, the molar extinction coefficient is 33% lower than those of the extended conjugation dyes (K-19 or K-73) in solution. In terms of the optical density of the adsorbed dyes on a 8 μm thick transparent film, there is a 35% decrease for Z 907Na dye over the K-73 or K-19 dyes (Figure S5). This result indicates that there is only a small change in the amount of adsorbed dyes on the film.

Excitations of the low energy MLCT transition of the K-73 dye in DMF solvent produces an emission centered at 830 nm (Figure S4). The emission spectrum was further analyzed by applying a Gaussian reconvolution method, which enabled determination of the integral under the emission peak, devoid of Raman and other instrumental artifacts. Knowledge on the formal redox potential of the excited state [$\phi^0(\text{S}^+/\text{S}^*)$] of a dye relative to the conduction band energy level of a TiO_2 semiconductor allows a priori determination of the direction of current flow. An approximate value of $\phi^0(\text{S}^+/\text{S}^*)$ of a dye can be extracted from the formal potential of the ground state [$\phi^0(\text{S}^+/\text{S})$] and its excitation energy (E_{0-0}) according to eq 1 (where F is the Faraday constant) obtained by electrochemical and spectroscopic measurements.

$$\phi^0(\text{S}^+/\text{S}^*) = \phi^0(\text{S}^+/\text{S}) - E_{0-0}/F \quad (1)$$

As presented in Figure S3, the formal redox potential of K-73 dye adsorbed on the surface of TiO_2 film obtained by averaging the anodic and cathodic peak potentials was 1.01 V vs NHE (normal hydrogen electrode). E_{0-0} transition energy was estimated to be 1.72 eV, and thus $\phi^0(\text{S}^+/\text{S}^*)$ of K-73 was calculated to be -0.71 V vs NHE.

The excited-state lifetimes of K-73 and K-19 were determined by transient absorbance measurements at 620 nm to be 24 ns and 12 ns, respectively (Figure S6). As the molar extinction coefficients of these two dyes are similar one expects the excited lifetimes to be close in value. These differences might have arisen due to the difference in the number of protons between K-19 and K-73 dyes. As the electron injection from the excited state dye is in the femtosecond range, the lifetime of the excited state measured is sufficient to produce quantitative injection of electrons into the TiO_2 electrodes.

2.3. ATR-FTIR Measurements. The spectrum of K-73 anchored on the mesoscopic TiO_2 film (Figure. S7) clearly shows the bands at 1624 cm^{-1} and 1380 cm^{-1} for the asymmetric and symmetric stretching modes of the carboxylate group and the complete loss of the 1717 cm^{-1} peak. From these ATR-FTIR data it can be inferred that the dye is anchored on the surface through the two carboxylate groups via a bidentate chelation or a bridging of surface titanium ions rather than an ester type linkage.¹³ The NCS group absorption remains at 2101 cm^{-1} indicating that the NCS coordinated to the ruthenium center through the N atom is unaffected by the adsorption process. The other peaks at 2847 cm^{-1} and 2924 cm^{-1} correspond to the stretching modes of the methyl while an sp^2 C-H stretching mode is observed at 3029 cm^{-1} . The sharp

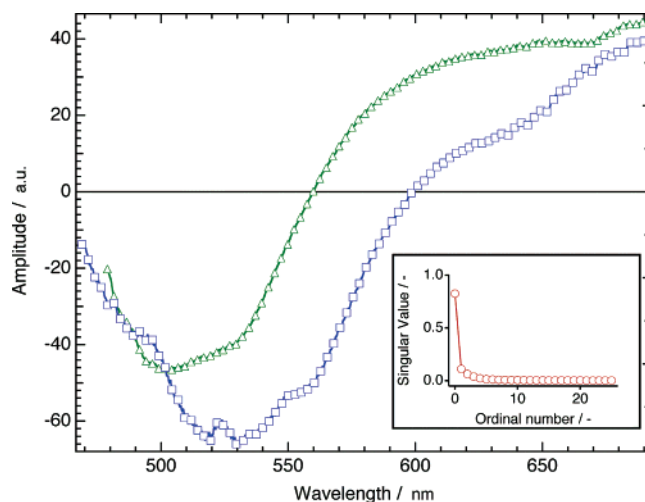


Figure 1. Base vector from the SVD of K19 observed on TiO_2 following excitation at 520 nm (\square) and on Al_2O_3 after excitation at 500 nm (Δ). The inset shows the singular values of the decomposition for the data obtained on TiO_2 (\circ).

peaks located at 1538 cm^{-1} and 1595 cm^{-1} arise from the aromatic ring modes.

3. Oxidized Form of the Sensitizer. The mesoscopic TiO_2 film of 6 μm thickness deposited on FTO glass was stained with a K-19 dye solution at room temperature for 16 h and used as a working electrode in a three electrode spectroelectrochemical cell. Acetonitrile was used as the solvent with TBA (PF_6) as the supporting electrolyte. The adsorbed monolayer of K-19 was oxidized by hole injection from the FTO support by applying a bias potential of 0.8 V vs NHE. Figure S8 shows the visible spectrum of the oxidized form of the K-19 sensitizer adsorbed on the mesoscopic TiO_2 film. Oxidation of K-19 results in bleaching of the low energy band at 545 nm with a growing feature centered at 775 nm. The weaker red shifted transition is assigned as a ligand-to-metal charge transition (LMCT) of the oxidized K-19 sensitizer. Previous investigations show that oxidation from ruthenium(II) to ruthenium(III) bipyridyl complexes results in a red shift in absorption and correspondingly weaker band intensities.¹⁴ From the absorption decay the half-life time of the oxidized K-19 sensitizer was determined as 2.6 min.

4. Ultrafast Electron Injection Kinetics. Time-resolved absorption changes were measured after excitation at 520 nm over a wavelength range extending from 470 to 690 nm. To get the best resolution for the temporal and spectral behavior, a singular value decomposition (SVD) was performed on the data matrix of which the rows and columns correspond to the single wavelength and time position vectors, respectively. This purely mathematical technique decomposes the initial matrix into two linearly independent bases and assigns a singular value to each of the base vectors. The number of nonzero singular values gives the rank of the matrix, i.e., in our case the number of the transient chemical species.¹⁵ The SVD of the measured transient data show clearly one dominating singular value suggesting that a single chemical species is present (see inset of Figure 1). The row vector associated with this value gives the spectral shape of this species. The profile of this transient

(13) Shklover, V.; Ovehinnikov, Y. E.; Braginsky, L. S.; Zakeeruddin, S. M.; Grätzel, M. *Chem. Mater.* **1998**, *10*, 2533.

(14) Nazeeruddin, M. K.; Zakeeruddin, S. M.; Kalyanasundaram, K. *J. Phys. Chem.* **1993**, *97*, 9607.

(15) Satzger, H.; Zinth, W. *Chem. Phys.* **2003**, *295*, 287.

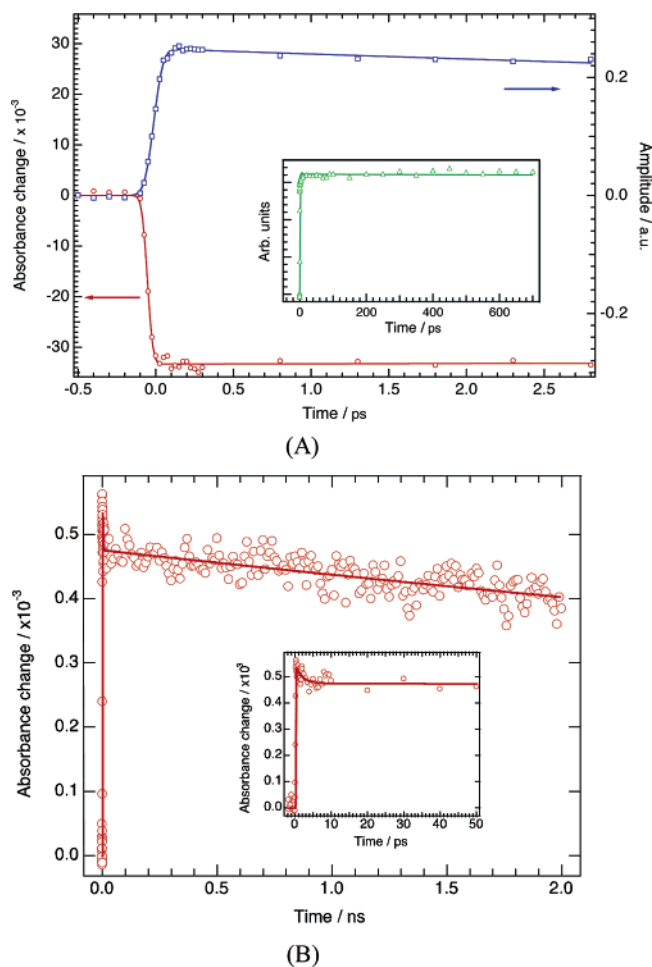


Figure 2. (A) Transient absorption on TiO_2 at 530 nm following excitation at 520 nm (\circ) and first base vector of the singular value decomposition (\square). The inset shows the time vector from an SVD realized on the data obtained with reduced laser pump fluence (\triangle). (B) Transient absorbance of K-19 adsorbed on a TiO_2 film in the presence of the nonvolatile electrolyte. The sample is probed at 890 nm upon excitation at 535 nm. The early-time dynamics are detailed in the inset. Data are fitted with the analytical convolution function of a Gaussian instrument response with two exponential decays, $\tau_1 = 1.9$ ps (12%) and $\tau_2 = 12$ ns (88%).

is almost exactly the same as the one obtained from detailed analysis of the analogue dye N3.¹⁶ The time vector associated to this component is given in Figure 2A.

The spectral shape and the time evolution of the unique transient species present after excitation of K-19 on TiO_2 indicates that it can be reasonably identified as the oxidized state of the dye. The same experiment was performed on Al_2O_3 in order to obtain information about the excited state. Since the conduction band edge potential of this material lies much higher than the energy levels populated in the excited state of the dye no electron injection is expected. Again an SVD was carried out, and a single transient species was identified. The spectral profile of the excited state is significantly different from the one observed on TiO_2 (Figure 1). Comparison with the electrochemically oxidized K-19 absorption spectra (Figure S8) allows us to assign the latter confidently to the photo-oxidation product of K-19. The fact that the transient spectrum of the oxidized state produced on TiO_2 is very similar to that of the

oxidized N3 dye corroborates that the transition responsible for the broad absorption band centered around 750 nm is a ligand-to-metal charge-transfer transition.

The rate of electron injection from K-19 into TiO_2 is illustrated in Figure 2A by the time vector associated to the spectral vector discussed above. The oxidized state appears to reach its maximum within the pulse duration. A small decay is apparent. It is imputed to a degradation of the dye rather than to recombination or any other chemical reaction since the bleaching observed at 530 nm does not evolve in the same way. This means that the ground state is not regenerated over the time range of our experiment (0–2000 ps). The degradation is likely to be due to the high pump intensities needed to get a good spectral resolution. When the intensity is reduced (<0.5 $\mu\text{J}/\text{pulse}$) the signal is perfectly stable, no evolution of the transient species is observed (see inset of Figure 2A). Cleavage of the C–S bond in the thiocyanate ligand as observed for N3 might be responsible for this behavior.^{16a} Data are fitted with an analytical convolution of a Gaussian function representing the instrument response with an exponential decay. The fitted full width at half-maximum (fwhm) of 70 fs allows us to give an upper limit for the electron-transfer time constant of 20 fs similar to the estimated value for deprotonated N3 in the absence of slow components related to dye aggregation on the semiconductor's surface.¹⁷

From the femtosecond time-resolved and spectrally resolved data we can conclude that electron injection from K-19 to TiO_2 's conduction band is ultrafast and therefore not expected to be hindered by any competitive process. In addition we observe that the spectral signature of the oxidized state of K-19 is identical to those of other N3 derivatives.

Very recently, Haque et al. reported that electron injection could be significantly slower in complete solar cells occurring with a half-life time of 150 ps.¹⁸ These authors suggested that the retardation was a consequence of the influence of the electrolyte upon the conduction band energetics of TiO_2 . To examine this possibility we performed two-color pump–probe transient absorption measurements of samples containing the nonvolatile electrolyte employed in highly stable solar cells for outdoor applications.^{8b} After light excitation at 535 nm, transient absorption was monitored at 890 nm where the contribution of the oxidized dye largely dominates the signal. As depicted in Figure 2B, no additional rise is observed after the pump pulse, indicating that injection is completed within the pulse duration, similar to the results obtained in the inert ionic liquid where no evolution is observed during the first nanoseconds. However, with the redox electrolyte, a biphasic decay is observed. The slower part in the nanosecond time scale is attributed to the diffusive regeneration of the oxidized dye by iodide. The faster component of the reduction reaction ($\tau = 1.9$ ps (12%)) is attributed to a static interaction between iodide and the ruthenium dye, the time constant associated with this process precluding diffusion of iodide.¹⁹

5. Dye Regeneration. Laser transient absorbance measurements were performed to understand the photon-to-current conversion efficiency of DSCs that is strongly dependent upon the kinetic competition between back electron transfer of injected

(16) (a) Moser, J. E.; Noukakis, D.; Bach, U.; Tachibana, Y.; Klug, D. R.; Durrant, J. R.; Humphry-Baker, R.; Grätzel, M. *J. Phys. Chem. B* **1998**, *102*, 3649. (b) Das, S.; Kamat, P. V. *J. Phys. Chem. B* **1998**, *102*, 8954.

(17) Wenger, B.; Grätzel, M.; Moser, J.-E. *J. Am. Chem. Soc.* **2005**, *127*, 12150. (18) Haque, S. A.; Palomares, E.; Cho, B. M.; Green, A. N. M.; Hirata, N.; Klug, D. R.; Durrant, J. R. *J. Am. Chem. Soc.* **2005**, *127*, 3456–3462.

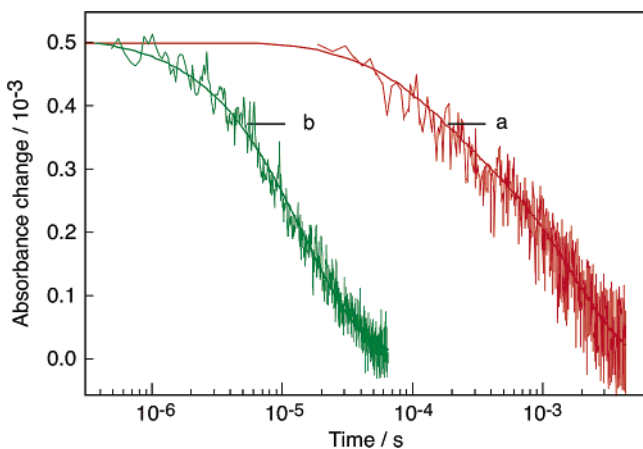
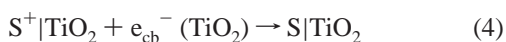
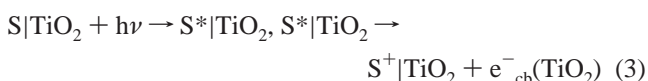


Figure 3. Transient absorbance decay kinetics of the oxidized state of K-19 dye, adsorbed on a mesoporous TiO₂ film in pure EMITFSI inert ionic liquid (a) and in the presence of present binary ionic liquid (PMII and EMINCS) electrolyte (b). The dye was coadsorbed from a solution in acetonitrile and *tert*-butyl alcohol (volume ratio: 1:1) containing PPA (1:1, molar ratio). Absorbance changes were measured at a probe wavelength of 680 nm, employing 600 nm laser excitation (5 ns fwhm pulse duration, 25 $\mu\text{J cm}^{-2}$ pulse fluence). Continuous lines drawn on top of experimental data are monoexponential fit curves with first-order rate constants $k = 1.4 \times 10^3 \text{ s}^{-1}$ (a) and $k = 1.1 \times 10^5 \text{ s}^{-1}$ (b), respectively.

electrons from the TiO₂ conduction band to the oxidized dye cations (S⁺) and the interception of S⁺ by the redox mediator. This efficiency is in fact directly proportional to the dye regeneration yield Φ_r , defined as

$$\Phi_r = k_r / (k_r + k_b) \quad (2)$$

In eq 2, k_r is the first-order rate constant of the dye regeneration (eq 5) occurring in the presence of a redox couple (D⁺/D), and k_b , the rate constant of the recombination reaction (eq 4) that takes place between the dye oxidized state S⁺ and the conduction band electron e_{cb}^- injected during the primary ultrafast photo-induced charge separation process (eq 3).



Hence, it is essential to scrutinize the dynamics of these charge-transfer processes with time-resolved nanosecond laser experiments.

Figure 3a shows the time evolution of the K-19 transient absorbance anchored on a mesoscopic transparent TiO₂ film in the presence of EMITFSI redox-inactive ionic liquid. In the absence of an electron donor, the decay of the transient absorption signal recorded at 680 nm following pulsed laser excitation reflects the dynamics of recombination of injected electrons with the oxidized dye (S⁺). The kinetics of S⁺ transient absorbance decay exhibited a typical half-life time of $t_{1/2} = 800 \mu\text{s}$ (Figure 3, trace a). In the presence of the binary ionic liquid (PMII and EMINCS) electrolyte, the decay of the oxidized dye signal was significantly accelerated with $t_{1/2} = 10 \mu\text{s}$ (Figure 3, trace b). The dye regeneration appeared to occur faster than

that of Z-907 in organic solvent electrolyte.²⁰ Remarkably, the regeneration reaction kinetics can be described by a single-exponential decay with a first-order rate constant $k_r = 1.1 \times 10^5 \text{ s}^{-1}$. Although data for the charge recombination kinetics could not be fitted accurately with a single-exponential decay, a rate constant of $k_b = 1.4 \times 10^3 \text{ s}^{-1}$ was approximated (Figure 3, trace a), leading to a dye regeneration yield of 99%.

6. Ionic Liquid Electrolytes, Effect of the Scattering Layer, and Film Thickness on Photovoltaic Performance. Strikingly high conversion efficiencies are obtained with the new sensitizers in full sunlight using ionic liquid (IL) electrolytes. Due to their high stability and negligible vapor pressure, these solvent-free redox systems play a key role for practical applications of the DSC. Advantage is taken of the enhanced optical cross section of the sensitizer to reduce the mesoscopic TiO₂ film thickness alleviating the mass transfer limitations of the photocurrent, which are notorious for ILs due to their high viscosity. Thus a K-19 stained TiO₂ layer of only 6.8 μm thickness used in combination with the binary ionic liquid electrolyte gave $J_{\text{sc}} = 12.15 \text{ mA cm}^{-2}$, $V_{\text{oc}} = 714 \text{ mV}$, $\text{FF} = 0.737$, and $\eta = 6.4\%$. This is an impressive performance for a solvent-free, transparent DSC. The conversion efficiency increased from 6.4 to 7.1% by adding a scattering layer of 4 μm thickness to augment the light harvesting in the red and near-IR region increasing the photocurrent.

Further insight in the behavior of the solvent-free DSC based on the new K-19 sensitizer was obtained by investigating the effects of film thickness and light intensity. Figure S9 shows the photocurrent response to a light on–off sequence produced by opening and closing a mechanical shutter that blocks the light beam. Under low light levels (<100 W/m²), the current remains constant on a time scale of seconds, while, for the thicker films, decay is noted when the intensity is raised to $\geq 300 \text{ W/m}^2$ indicating a mass transport limitation of the photocurrent under these conditions. Thinner films made of a 3.4 or 6.8 μm thick colloidal layer and a superimposed 4 μm thick scattering layer gave the best performance with the binary ionic liquid electrolyte.

Figure 4 and Table 1 show the effect of varying the colloidal TiO₂ particle layer thickness on the photovoltaic parameter (J_{sc} , V_{oc} , FF , η) keeping the 4 μm reflecting particle layer constant and using K-19 sensitizer coadsorbed with PPA. The V_{oc} decreases with increasing film thickness, due to the augmentation of the surface area providing additional charge-recombination sites and enhancing the dark current. Moreover, for thicker films the outer TiO₂ particle layers do not contribute significantly to the photogeneration of conduction band electrons due to the filtering of light by the dyed particles located close to the FTO glass. The sharing of photoinjected conduction band electrons by these particles lowers their quasi-Fermi level and hence the V_{oc} . By contrast, both J_{sc} and η peaked at 6.8 μm , while the fill factor remained constant.

Electron transport and recombination in TiO₂ particles and at the TiO₂/redox electrolyte interface have been investigated by using various experimental techniques such as IMPS, IMVS,

- (19) Marton, C.; Clark, C. C.; Srinivasan, R.; Freundlich, R. E.; Narducci Sarjeant, A. A.; Meyer, G. J. *Inorg. Chem.* **2006**, *45*, 362–369.
 (20) Wang, P.; Zakeeruddin, S. M.; Moser, J. E.; Nazeeruddin, M. K.; Sekiguchi, T.; Grätzel, M. *Nat. Mater.* **2003**, *2*, 402.

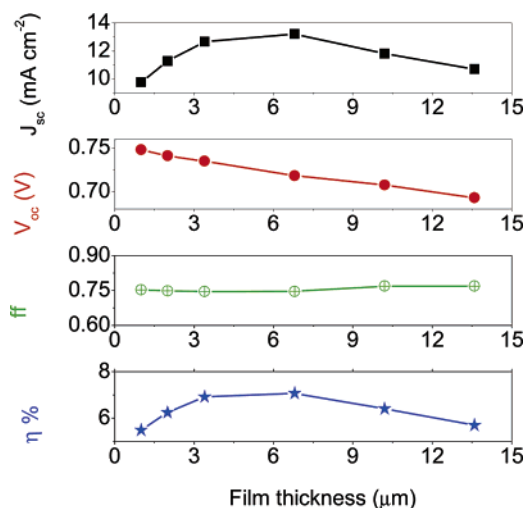


Figure 4. The detailed photovoltaic parameter (J_{sc} , V_{oc} , FF, and η) variations with different film thicknesses of transparent layer and keeping constant $4 \mu\text{m}$ reflecting layer based on K-19 dye, and PPA as coadsorbent and ionic liquid electrolyte.

Table 1. Detailed Photovoltaic Parameters (J_{sc} , V_{oc} , FF, and η) for Different Film Thicknesses Based on K-19 Dye and PPA as Coadsorbent with a Solvent-Free Ionic Liquid Electrolyte

film thickness (μm)	J_{sc} (mA/cm^2)	FF	V_{oc} (mV)	efficiency (%)
1 + 4	9.75	0.752	747.87	5.49
2 + 4	11.26	0.748	740.98	6.25
3.4 + 4	12.65	0.745	734.67	6.92
6.8 + 4	13.2	0.746	718.08	7.07
10.2 + 4	11.8	0.768	707.4	6.41
13.6 + 4	10.68	0.768	692.89	5.7

photocurrent transient, and EIS.^{2,21–29} Changes in the TiO_2 film thickness could affect these important properties.³⁰ Electrochemical impedance studies were performed to further elucidate these factors for the present ionic liquid electrolyte system.

7. Electrochemical Impedance Spectroscopy Studies. Electrochemical impedance spectroscopy (EIS) is a powerful tool for identifying electronic and ionic transport processes in DSC. Adequate physical models and equivalent circuits have been

proposed and applied to analyze the electron transport in TiO_2 film and recombination at the $\text{TiO}_2/\text{electrolyte}$ interface in DSC.^{26–29} The EIS investigation of the DSC device provides valuable information for the understanding of photovoltaic parameters (J_{sc} , V_{oc} , FF, and η). Impedance spectra of DSC devices with different film thicknesses ($1 + 4$, $6.8 + 4$, and $13.6 + 4 \mu\text{m}$) used in conjunction with the K-19 dye and the above-mentioned binary ionic liquid electrolyte were measured under one sun illumination at an open circuit potential or in the dark at -0.68 V , shown in Figure 5. A typical EIS spectrum exhibits three semicircles in the Nyquist plot or three characteristic frequency peaks in a Bode phase angle presentation as indicated in Figure 5. In the order of increasing frequency the features are attributed to the Nernst diffusion in the electrolyte, electron transfer at the $\text{TiO}_2/\text{electrolyte}$ interface, and redox charge transfer at the counter electrode, respectively. The features for electron transport in the TiO_2 film and interfacial recombination overlap in the frequency range from 10^2 to 10^3 Hz .

The chemical capacitance (C_{μ}) and charge-transfer resistance (R_{ct}) were obtained by fitting the middle frequency semicircle in the Nyquist plots. The C_{μ} , which is scaled to the film thickness, and R_{ct} , which is scaled to the inverse of the film thickness, is shown in Figure S10. Under light illumination, we see that the R_{ct} has no obvious change with the inverse of the film thickness. Since C_{μ} has a near linear relationship with film thickness, this resulted in the shift of a characteristic peak to lower frequency with an increase in the film thickness. In the dark, the capacitance increases linearly with film thickness (d) and the R_{ct} decreases linearly to $1/d$, resulting in an almost constant response time. In both cases, when measured under light at an open circuit potential (Figure 5a) or in the dark at -0.68 V (Figure 5c), the diffusion of I_3^- ion in the electrolyte slows down with an increase in film thickness shifting the lowest frequency peak in the Bode plot to smaller values. This trend also can be seen by the Nyquist plots (Figure 5b and 5d). The electron diffusion time also increases with film thickness as shown by the shift of the main peak in the 10^2 to 10^3 Hz range of the Bode plot to lower frequencies. The Warburg diffusion resistance for electron motion becomes clearly visible for the thickest film at the high-frequency end of the corresponding semicircle in the Nyquist presentation.

This observation is rationalized in terms of an increase in the number of traps encountered by the conduction band electrons with increasing film thickness. This slows down the electron motion lowering the electron collection efficiency. From the $I-V$ data in Table 1, the current density augments only 30%, i.e., from 9.8 mA cm^{-2} to 13 mA cm^{-2} upon increasing the thickness of the transparent layer 6.8 times, i.e., from $1 \mu\text{m}$ to $6.8 \mu\text{m}$. Thereafter, the current density actually decreases with film thickness up to $13.6 \mu\text{m}$ despite enhanced light absorption, which can be explained by slow electron diffusion and consequently low electron collection efficiency.

8. Photovoltaic Performance. The photocurrent action spectrum of the device coadsorbed with K-73 and DPA in combination with a nonvolatile electrolyte is shown in Figure 6. The incident photon to current conversion efficiency (IPCE) exceeds 70% in a spectral range from 470 to 620 nm, reaching its maximum of 85% at 540 nm. Considering the light absorption and scattering loss by the conducting glass, the maximum

- (21) (a) Dloczik, L.; Ieperuma, O.; Lauermaun, I.; Peter, L. M.; Ponomarev, E. A.; Redmond, G.; Shaw, N. J.; Uhlendorf, I. *J. Phys. Chem. B* **1997**, *101*, 10281. (b) Schlichthörl, G.; Huang, S. Y.; Sprague, J.; Frank, A. J. *J. Phys. Chem. B* **1997**, *101*, 8141. (c) Oekermann, T.; Yoshida, T.; Minoura, H.; Wijayantha, K. G. U.; Peter, L. M. *J. Phys. Chem. B* **2004**, *108*, 8364.
- (22) Kern, R.; Sastrawan, R.; Ferber, J.; Stangl, R.; Luther, J. *Electrochim. Acta* **2002**, *47*, 4213.
- (23) (a) Frank, A. J.; Kopidakis, N.; van de Lagematt, J. *Coord. Chem. Rev.* **2004**, *248*, 1165. (b) Nakade, S.; Kanzaki, T.; Kubo, W.; Kitamura, T.; Wada, Y.; Yanagida, S. *J. Phys. Chem. B* **2005**, *109*, 3480.
- (24) Solbrand, A.; Lindström, H.; Rensmo, H.; Hagfeldt, A.; Lindquist, S. E. *J. Phys. Chem. B* **1997**, *101*, 2514.
- (25) (a) Schwarzbarg, K.; Willig, F. *J. Phys. Chem. B* **2003**, *107*, 3552. (b) Zaban, A.; Meier, A.; Gregg, B. A. *J. Phys. Chem. B* **1997**, *101*, 7985.
- (26) Bisquert, J. *J. Phys. Chem. B* **2002**, *106*, 325.
- (27) (a) Bisquert, J. *J. Phys. Chem. Chem. Phys.* **2003**, *5*, 5360. (b) van De Lagematt, J.; Park, N. G.; Frank, A. J. *J. Phys. Chem. B* **2000**, *104*, 2044. (c) Bisquert, J.; Zaban, A.; Greenshtein, M.; Mora-Sero, I. *J. Am. Chem. Soc.* **2004**, *126*, 13550.
- (28) Fabregat-Santiago, F.; Bisquert, J.; Garcia-Belmonte, G.; Boschloo, G.; Hagfeldt, A. *Solar Energy Materials & Solar Cells* **2005**, *87*, 117.
- (29) Wang, Q.; Moser, J. E.; Grätzel, M. *J. Phys. Chem. B* **2005**, *109*, 14945.
- (30) (a) Nazeeruddin, M. K.; Kay, A.; Rodicio, I.; Humphry-Baker, R.; Müller, E.; Liska, P.; Vlachopoulos, N.; Grätzel, M. *J. Am. Chem. Soc.* **1993**, *115*, 6382. (b) Kang, M. G.; Ryu, K. S.; Chang, S. H.; Park, N. G.; Hong, J. S.; Kim, K. J. *Bull. Korean Chem. Soc.* **2004**, *25*, 742. (c) Park, N. G.; van de Lagematt, J.; Frank, A. J. *J. Phys. Chem. B* **2000**, *104*, 8989. (d) Ito, S.; Kitamura, T.; Wada, Y.; Yanagida, S. *Solar Energy Materials & Solar Cells* **2003**, *76*, 3.

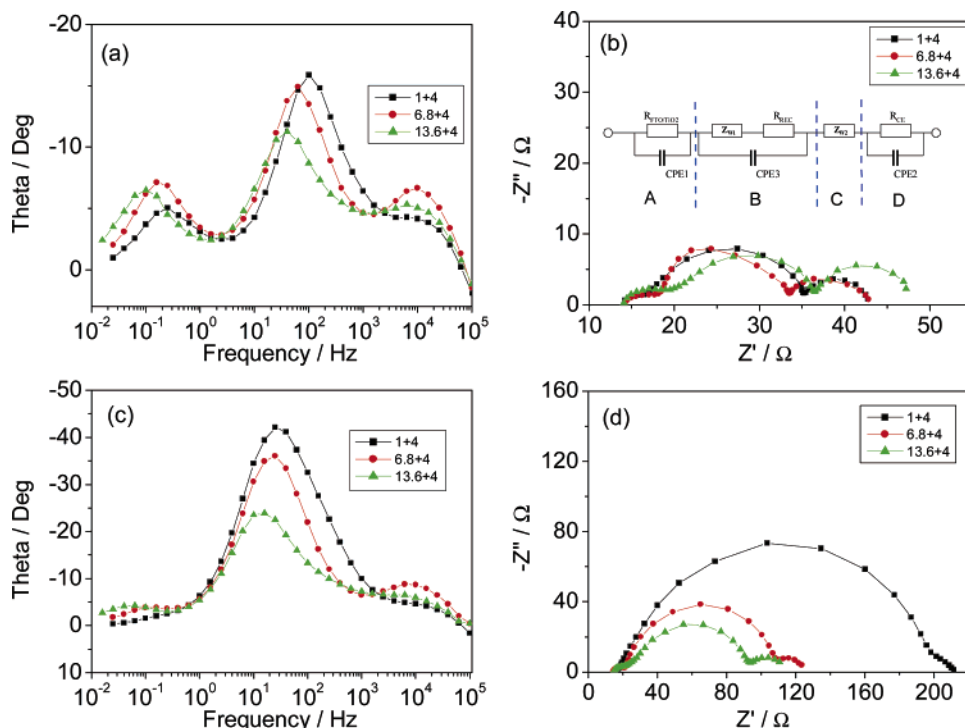


Figure 5. Impedance spectra of DSC devices based on different film thickness measured under 1 sun illumination at open circuit potential (a, b) or in dark at a forward bias of -0.68 V (c, d). Bode phase plots: (a) and (c); Nyquist plots: (b) and (d). Black: $(1 + 4)$ μm film. Red: $(6.8 + 4)$ μm film. Green: $(13.6 + 4)$ μm film. The inset of Figure 5b is the equivalent circuits of DSC.²⁹ (A) electron transfer at the FTO/TiO₂ interface; (B) electron transport and back reaction at the mesoscopic TiO₂/electrolyte interface; (C) diffusion of I₃⁻ in the electrolyte; (D) charge transfer at the electrolyte/Pt–FTO interface.

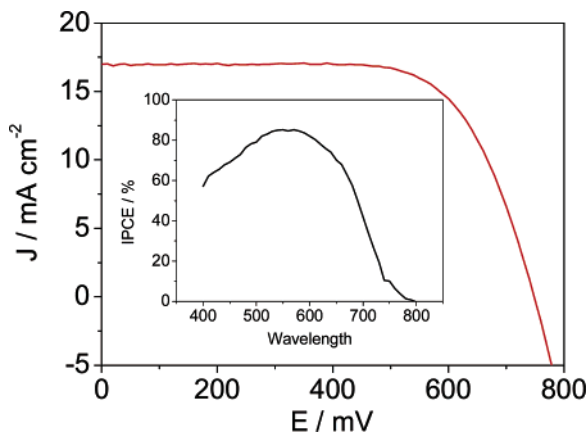


Figure 6. Photocurrent density–voltage curves of the DSC device based $(6.8 + 4)$ μm film sensitized with K-73/DPA and nonvolatile electrolyte under AM 1.5 full sunlight (100 mW cm^{-2}). The inset is the photocurrent action spectra of the same DSC device. Cell active area: 0.158 cm^2 .

efficiency for absorbed photon to current conversion efficiency is practically unity over this spectral range. As shown in Figure 6, the short-circuit photocurrent density (J_{sc}), open-circuit photovoltage (V_{oc}), and fill factor (FF) of the K-73 dye based device under AM 1.5 full sunlight are 17.22 mA cm^{-2} , 748 mV , and 0.694 , respectively, yielding an overall conversion efficiency (η) of 9% . At lower light intensities, the overall power conversion efficiencies are over 9.5% . These are the highest conversion efficiencies ever reported for DSCs based on nonvolatile electrolytes. It is important to note that this impressive performance is achieved with thin films, the nanocrystalline TiO₂ layer being only 6.8 microns thick, vindicating our approach for developing heteroleptic high extinction coefficient sensitizers.

Table 2. Detailed Device Parameters Based on $(6.8 + 4)$ μm TiO₂ Double Layer Film Sensitized with K-19/PPA and Using Ionic Liquid Electrolyte under Various Incident Light Intensities^a

P_{in} (mW/cm^2)	J_{sc} (mA/cm^2)	V_{oc} (mV)	P_{max} (mW/cm^2)	FF	η (%)
99.4	13.2	718	7.0	0.746	7.1
51.7	7.4	703	4.0	0.789	7.8
30	4.3	688	2.4	0.802	8.0

^a P_{in} : Incident power intensity. J_{sc} : Short-circuit photocurrent density. V_{oc} : Open-circuit photovoltage. P_{max} : Maximum electrical output power density. FF: Fill factor ($\text{FF} = P_{\text{max}}/P_{\text{in}}$). η : Total power conversion efficiency. Cell active area tested with mask: 0.158 cm^2 . The spectral distribution of the lamp (incident light source) simulates air mass 1.5 solar light.

The photovoltaic parameters (V_{oc} , J_{sc} , and FF) of the device prepared with a $6.8 + 4$ μm film and K-19 dye coadsorbed with PPA in combination with a solvent-free ionic liquid electrolyte are 718 mV , 13.2 mA cm^{-2} , 0.745 , respectively, yielding an overall efficiency (η) of 7.1% . It is worth noting that the photoelectric conversion efficiency reached as high as 8.0% under an irradiance of 30 mW cm^{-2} . The detailed parameters (J_{sc} , V_{oc} , FF, and η) of the device under different light intensities are shown in Table 2.

The aim of designing high molar extinction coefficient sensitizers is to obtain high efficiencies with thinner mesoscopic TiO₂ films. To demonstrate that this strategy works, we chose for comparison the Z-907Na dye which has a 33% lower molar extinction coefficient than that of K-19 dye, by using a 3.4 μm transparent TiO₂ film in combination with a binary ionic liquid electrolyte. Using the K-19 dye we obtained a 19% higher current density (10.9 mA cm^{-2}) than measured with Z-907Na (8.8 mA cm^{-2}) at full sun irradiance resulting in an overall efficiency increase of 20% (from 5% to 6%). This result

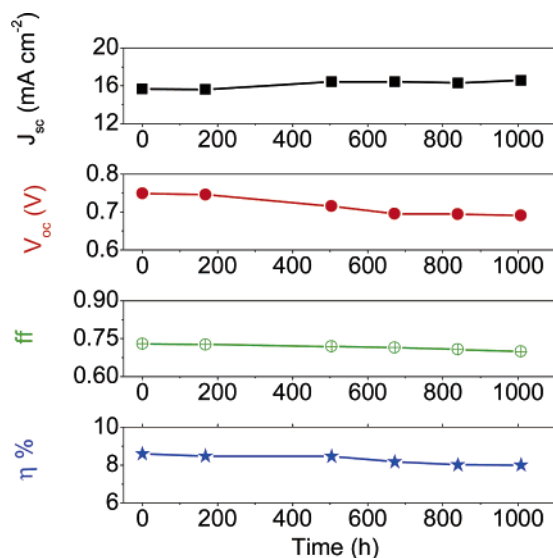


Figure 7. Photovoltaic parameter (J_{sc} , V_{oc} , FF, and η) variations with aging time for the device based on $(6.8 + 4) \mu\text{m}$ film sensitized with K-73/DPA and nonvolatile electrolyte during successive one sun visible-light soaking at 60°C .

undoubtedly demonstrates the advantage of high extinction coefficient sensitizers in DSC.

9. Device Stability. The K-73 dye showed good stability when subjected during 1000 h to light soaking at 60°C in the solar simulator (Figure 7). However during long term heating at 80°C a desorption of the sensitizer from the surface was noted. In contrast, the K-19 dye showed excellent stability under both light soaking at 60°C and thermal stress at 80°C .⁸ Thus it appears that the adsorption of the sensitizer is strengthened by the presence of the long alkyl chains on the K-19 dye, producing high thermal stability in the presence of the non-volatile electrolyte employed here.

Devices employing K-19 in conjunction with ionic liquid electrolytes showed also excellent long-term stability, when subjected to an accelerated light soaking test at 60°C . Figure 8 presents the stability data of the device containing K-19 dye and PPA as coadsorbent which kept 93% of the initial performance after the 1000 h light soaking test. It is worth noting that after a week of light soaking at 60°C the efficiencies of DSC at full sun and 0.3 sun illumination increased to 7.3% and 8.3%, respectively. After 1000 h of light soaking, the V_{oc} decreased by 60 mV but this loss is compensated by a gain in short circuit current density from 13.2 to 14.5 mA cm^{-2} . The long-term stability of the device at low light intensity (0.3 sunlight) is even better than 1 sunlight intensity; the initial efficiency of 8.0% is decreased to 7.8% during the 1000 h light soaking test. The use of the novel high extinction coefficient sensitizers in conjunction with ionic liquid appears to also provide stability advantages at low light intensities.

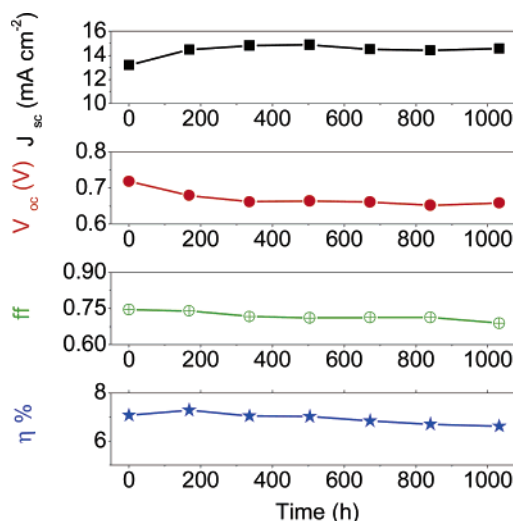


Figure 8. Photovoltaic parameter (J_{sc} , V_{oc} , FF, and η) variations with aging time for the device based on $(6.8 + 4) \mu\text{m}$ film sensitized with K-19/PPA and ionic liquid electrolyte during successive one sun visible-light soaking at 60°C .

Conclusions

The present study confirms the advantage of high extinction coefficient sensitizers in realizing efficient thin film solar cells. The two novel high molar extinction coefficient ruthenium dyes with (K-19) and without amphiphilic chains (K-73) presented show very attractive features with regards to photovoltaic performance and stability. Devices based on the K-73 dye and a nonvolatile electrolyte yielded an unprecedented overall conversion efficiency of 9% under AM 1.5 global sunlight. Solar cells employing the K-19 dye in combination with a binary ionic liquid electrolyte gave over 7.0% efficiency and maintained excellent stability under light soaking at 60°C for 1000 h. Work is in progress to enhance further the photovoltaic performance and long-term stability of DSCs based on nonvolatile or solvent-free ionic liquid electrolytes for which practical applications can be foreseen soon.

Acknowledgment. We are grateful to Dr. Qing Wang and Dr. Augustin McEvoy for helpful discussions, P. Comte and R. Charvet for the mesoscopic TiO_2 paste fabrication, T. Koyanagi (CCIC, Japan) for providing the 400 nm sized TiO_2 particles, and The Swiss Science Foundation and Swiss Federal Office for Energy (OFEN) which have supported this work.

Supporting Information Available: Detailed characterizations of K73 dye, device photocurrent transient, film capacitance, and charge-transfer resistance for different film thickness. This material is available free of charge via the Internet at <http://pubs.acs.org>.

JA058540P